IEEE Open Access Journal of Power and Energy

Received 3 October 2021; revised 14 May 2022; accepted 18 May 2022.
Date of publication 1 June 2022; date of current version 14 June 2022.

Digital Object Identifier 10.1109/OAJPE.2022.3179453

Evaluation Tests of Metal Oxide Varistors for DC Circuit Breakers

CHUNMENG XU[1] (Member, IEEE), ANDREW ROCKHILL[2] (Senior Member, IEEE), ZHI JIN ZHANG[1] (Graduate Student Member, IEEE), MATTHEW BOSWORTH[3] (Member, IEEE), MARYAM SAEEDIFARD[1] (Fellow, IEEE), MICHAEL STEURER[3] (Senior Member, IEEE), PETER ZELLER[3] (Senior Member, IEEE), AND LUKAS GRABER[1] (Senior Member, IEEE)

[1]Department of Electrical and Computer Engineering, Georgia Institute of Technology, Atlanta, GA 30332 USA
[2]Eaton Research Labs, Milwaukee, MI 53051 USA
[3]Center for Advanced Power Systems, Florida State University, Tallahassee, FL 32310 USA
CORRESPONDING AUTHOR: C. XU (chunmengxu@gatech.edu)

This work was supported in part by the U.S. Office of Naval Research under Contract N00014-14-C-0123 and in part by the U.S. Advanced Research Projects Agency–Energy Agency under Grant DE-AR0001113.

ABSTRACT With emerging technologies and products in power semiconductors and ultrafast mechanical switches, direct-current circuit breakers (DCCBs) have been developing rapidly. Yet the metal-oxide varistors (MOVs), being the indispensable DCCB components, are less analyzed and tested so far. Generally, MOVs in DCCBs are used to dissipate energy and limit overvoltage surges during switching events. This emerging application of MOVs calls for new design procedures and evaluation tests to ensure MOV performance under non-standard stresses and repetitive energy pulses. In this paper, online-monitored stress endurance tests are performed on MOVs that are employed in a 12 kV DCCB. Most MOVs have endured the DCCB-derived stresses for about 3500 pulses with little variation in their voltage-current characteristics, while only one fails after 1000 pulse tests and gets damaged by a shunt conductive channel. Different from conventional operating points of MOVs in their voltage-current characteristics, the MOVs in DCCB applications are found to work routinely in the temporary overvoltage (TOV) region with a decreasing TOV current over time. As these behaviors of MOVs are scarcely reported in the literature or covered by their datasheets, this study presents one of the first publicly available endurance test data that address the knowledge gaps about energy-dissipating MOVs in switchgear applications.

INDEX TERMS Direct-current circuit breaker (DCCB), hybrid circuit breaker (HCB), solid-state circuit breaker (SSCB), surge arrester, temporary overvoltage, high-voltage direct-current (HVDC), metal-oxide varistor.

I. INTRODUCTION

METAL-OXIDE varistors (MOVs) have been widely chosen as energy dissipation devices in direct-current switchgear applications like solid-state circuit breakers (SSCBs) [1]–[3] and hybrid circuit breakers (HCBs) [4]–[6]. Given the distinguished energy absorption capability in medium-voltage MOVs, like several kilojoules per kilovolt of rated voltage [7], repetitive absorption of excessive energy is still a ''lifetime-threatening'' process that may cause overheating, nonlinear degradation, and mechanical failure in a MOV structure [8]–[10]. Not to mention the switching energy during circuit interruptions in high-voltage direct-current (HVDC) circuit breakers can be enormous, which is reported as high as 2 MJ per switching event [11].

The MOVs in DCCBs are subject to DC switching waveforms that are fundamentally different from lightning-derived waveforms specified in the industrial standards [11], [12]. Prior to DCCB applications, MOVs have been used as overvoltage suppressors against lightning-induced and switching-induced overvoltage in power systems for decades [13], [14]. The lifetime of MOVs as overvoltage suppressors is thus evaluated with lightning-derived waveforms like 8/20 μs current impulse [7], [15], [16] and 2 ms rectangular waveforms [15, 17]. The current de-rating curves provided in the MOV

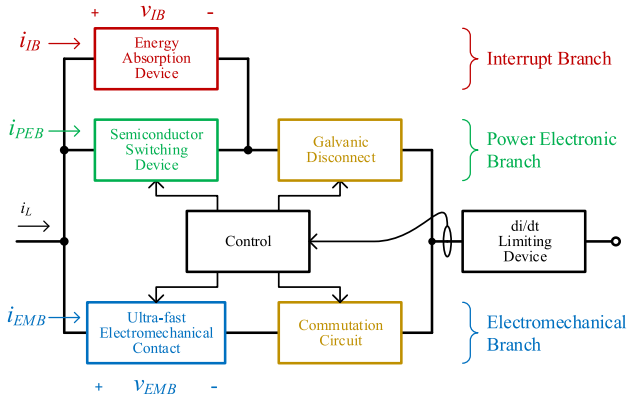

FIGURE 1. The exemplary structure of a hybrid circuit breaker (HCB) equipped with a commutation circuit in its electromechanical branch and a galvanic disconnect contactor in its power electronic branch.

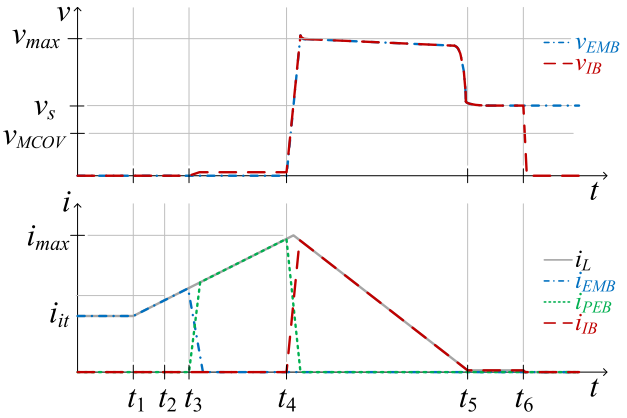

FIGURE 2. Voltage and current waveforms through electromechanical branch (v_{EMB}, i_{EMB}), power electronic branch (i_{PEB}) and interrupt branch (v_{IB}, i_{IB}) in the HCB during circuit-breaking processes.

datasheets are measured with a pseudo-rectangular current impulse [18], [19].

Inevitably, the aforementioned lightning-derived or pseudo-rectangular waveforms deviate considerably from DCCB-generated waveforms [20], [21]. If a MOV is selected according to its energy absorption capability based on 8/20 μs current impulses, it may not exhibit the same energy absorption capability under those DCCB-generated waveforms with different waveshapes, as the failure probability of the MOV depends on its loading stresses [22]. Therefore, the major innovative contributions of this paper include using the DCCB-derived waveforms for evaluating MOV endurances under repetitive stresses, discovering the unique operating points of MOVs in the temporary overvoltage (TOV) region, and summarizing the tendency of TOV current with time and temperature in MOVs under test. All above contributions are achieved with the automated test setup and the interleaved test procedures, which will be described thoroughly in following sections.

In this paper, the voltage and current waveforms derived from DCCB fault interruption processes are used to test the stress endurance of MOVs. The test setup, experimental procedures, and the unique operating points of MOVs in DCCB applications are presented. This study aims to optimize the expected lifetime of MOVs as energy absorbers in DCCB applications. In this way, the overall DCCB can achieve higher operational reliability and a longer lifetime expectancy.

The rest of this paper is structured as follows. Section II discusses the unique operating points of MOVs in DCCB applications. Section III presents a comprehensive test setup for online-monitored stress endurance tests with illustrations of DCCB-derived test waveforms. Section IV analyzes experimental results from pulse current and temporary overvoltage tests. Section V provides detailed failure analyses with physical inspections of the only MOV that did not pass the endurance tests. Section VI concludes this paper.

II. DCCB OPERATIONS WITH MOVs

A. DCCB WAVEFORMS

An exemplary structure of an HCB is shown in Fig. 1, which consists of an electromechanical branch to conduct nominal current, a power electronic branch to commute current, and an interrupt branch with MOVs to absorb energy and achieve circuit interruption. Eliminating the electromechanical branch in Fig. 1 gives an illustrative structure of an SSCB [23].

Fig. 2 illustrates the typical voltage and current waveforms during HCB current-interrupting process [24], [25]. According to Fig. 2, both the interruption branch voltage v_{IB} and the interruption branch current i_{IB} are initially zero before the current is commuted into the interruption branch at t_4. Between t_4 and t_5, MOVs attenuate the current pulse i_{IB} down to zero by converting the electrical energy into thermal energy like nonlinear resistors. Meanwhile, a maximum transient interruption voltage v_{max} is generated by MOVs between t_4 and t_5. Considering that v_{max} can be 1.5–2.5 times of the maximum continuous operating voltage (MCOV) of the MOVs [3], [26], special attention must be paid to ensure that it stays lower than the breakdown voltage of power electronic branch for protecting the semiconductor switching devices [27]. A common practice in DCCB prototypes is to use MOVs with slightly lower MCOV values than system voltage v_s, so that their maximum clamping voltage v_{max} is reduced accordingly to match up with the breakdown voltage of semiconductor switches [28], [29]. In this study, the MCOV values of MOVs are selected to be 2.2 kV, and their maximum clamping voltage is around 5 kV so that the 5.5 kV insulation limit of 4 kV-rated semiconductor modules in the DCCB prototype will not be violated. At the same time, the system voltage v_s of 4 kV becomes an "overvoltage" for the MOVs with 2.2 kV of MCOV values.

A considerable amount of temporary overvoltage (TOV) current will flow through MOVs after t_5 when the line voltage stabilizes at system voltage v_s, which may cause excessive power loss and overheating problems in MOVs. In order to

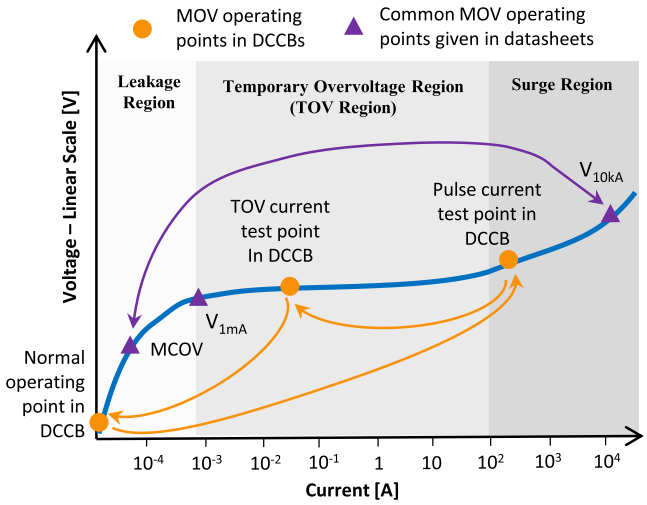

FIGURE 3. Nonlinear $V-I$ characteristic curve with datasheet-given parameter (MCOV, V_{1mA}, V_{10kA}) for MOVs as overvoltage suppressors, and the operating points for MOVs in the DCCB prototype of this study. The arrows indicate the transitional sequence of MOV operating points. The MOV voltage and current during DCCB operations may not exactly follow its $V-I$ characteristic curve.

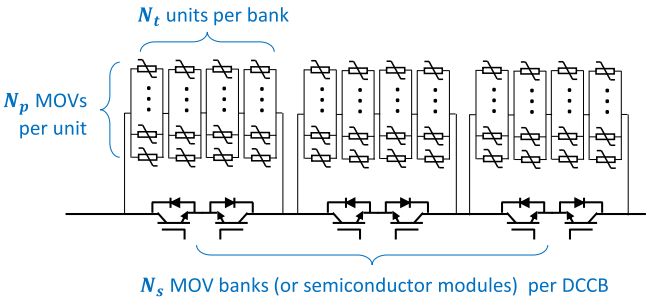

FIGURE 4. Circuit diagram of the interconnected MOVs in DCCBs.

TABLE 1. Design parameters of the DCCB prototype.

Component	Voltage Rating
DCCB	12 kV
IGBT	4 kV nominal, 5.5 kV insulation
MOV	2.2 kV MCOV, 5 kV clamping voltage

protect MOVs from overheating, a galvanic disconnect contactor in the power electronic branch of DCCB will cut off the TOV current at t_6 and reduce the v_{IB} down to zero. It must be ensured that the galvanic disconnect contactor can interrupt this small TOV current that ranges from a few milliamps to a few amperes under DCCB voltage rating. A medium-voltage vacuum interrupter has been selected for the 12 kV DCCB prototype in this study.

B. MOV OPERATING POINTS

Due to the significant differences between DCCB-derived stress waveforms in Fig. 2 and the lightning-derived impulses like the 8/20 μs overcurrent impulses, the MOVs in DCCBs have their unique operating points that deviate considerably from datasheet-given parameters as illustrated in Fig. 3.

Starting from the leakage region on the low-current side of Fig. 3, the normal operating point of MOVs in DCCBs is very close to the origin of $V-I$ characteristic curve because the applied voltage over MOVs is almost zero during DCCB normal operations. For example, the MOVs are bypassed while the DCCB is conducting line current (i_L in Fig. 1). The MOVs are also isolated by the galvanic disconnect contactor while the DCCB is fully switched off. Therefore, the MOVs in DCCBs are energized only for a short period of time during DCCB switching events. On the opposite, the MOVs installed in classical line-to-ground configurations for overvoltage protections are subject to system line-to-ground voltage continuously. For sustaining a low leakage current through line-to-ground-installed MOVs, their MCOV values must be selected to be equal to or larger than the system voltage, which is different from MCOV rating selection criteria for MOVs in DCCB prototypes.

The most unique operating point of MOVs in DCCBs resides in the TOV region of $V-I$ characteristic curve in Fig. 3. The TOV region is an intermediate, transitional area that could only be entered temporarily during MOV operations, otherwise, the TOV current will overload the MOV and cause overheating problems [10], [30]. The behaviors of MOVs within this TOV region are thus less investigated than the other two regions in literature [30]. However, the MOVs in DCCBs must stay in the TOV region during switching events (t_5 to t_6) before being cut off by the galvanic disconnect contactor. The time duration from t_5 to t_6 can be up to 100 ms in the DCCB prototype of this study. Therefore, the behaviors of MOVs in the TOV region must be carefully evaluated in this study.

In the surge region of $V-I$ characteristic curve, each MOV in the same DCCB deals with a smaller amount of current at its pulse current operating point [11], [28], [29], which is different from the datasheet-referred scenario that a single MOV discharging the whole 10 kA-peak impulse current. In this way, the interconnection of MOVs like Fig. 4 can achieve a higher energy absorption capability by distributing the surge current among parallel-connected MOVs. Nevertheless, it brings up a problem about the unbalanced current sharing, which leads to unequal stresses and consequently, unequal aging. In order to eliminate the variances of degradation caused by the unbalanced current sharing among parallel-connected MOVs in this study, the MOV specimens are tested individually in the endurance test setup as shown in Fig. 5. Specifically, the 12 kV-rated DCCB prototype of this study uses 36 MOVs in total. Referring to Fig. 4, there is a bank of 12 MOVs ($N_p = 12$, $N_t = 1$) with 2.2 kV of MCOV values being connected in parallel to one IGBT module which operates at 4 kV. As shown in Fig. 4, there are three IGBT modules ($N_s = 3$) being connected in series for this 12 kV DCCB prototype. The above design parameters have been summarized in Table 1.

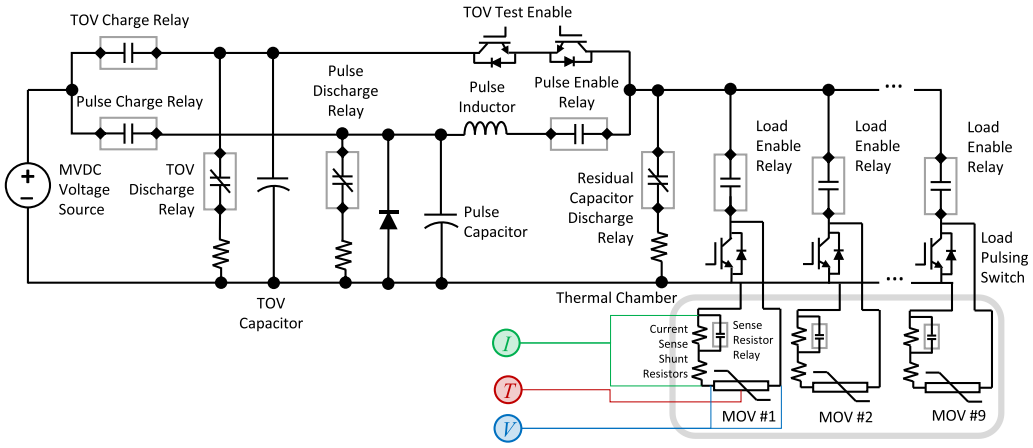

FIGURE 5. Circuit diagram of a co-located, fully-automated testbed for both pulse endurance tests and TOV current tests on nine MOV specimens. The MOVs are tested individually to minimize the variances in degradations caused by the unbalanced current sharing among parallel-connected MOVs.

III. ENDURANCE TEST SETUP AND PROCEDURES

A. TEST SETUP OVERVIEW

A comprehensive test circuit that can replicate the same pulse stresses and TOV stresses from DCCB circuit-breaking events is shown in Fig. 5. A practical challenge in the implementation of such a test circuit was to fit the largest number of MOVs, sensors, and fixtures inside an environmentally controlled chamber. The MOVs were thus separated far from the rest of test circuit as shown in Fig. 5 and Fig. 6(a). In order to reduce the loop inductance within the test circuit, tightly-coupled busbars were used to connect between an array of nine IGBT pulsing switches outside the chamber and an array of nine MOVs inside the chamber.

For the voltage measurement over individual MOVs during high di/dt events, two tightly-coupled high-voltage signal wires were brought out of the thermal chamber and interfaced with a high-bandwidth differential amplifier. The outputs of nine differential amplifiers were merged to a coaxial multiplexer (NI PXI 2593, 500MHz bandwidth) so that only the voltage waveform of the MOV-under-test was recorded and shown in the oscilloscope.

For the temperature measurement of each device, there were 18 medium-voltage isolated thermocouples, two for each MOV, embedded into MOV mounting clamps as shown in Fig. 6(b). The thermocouple signals were conditioned by four dedicated data loggers (Advantech ADAM 601x module) for data acquisitions.

For the current measurements during high dv/dt events, current shunt resistors were directly installed on the MOV mounting clamps within the thermal chamber. These current shunt resistors only measured the current flowing through the MOV, which eliminated the parasitic charging current due to inter-busbar capacitances. For the low-current leakage tests, a 1.0 ohm, 5% shunt resistor (KOA Speer BPR58CF1R0J) was connected in series with two paralleled 0.05 ohms 1% high-current shunt resistors (Ohmite TGHGCR0500FE) for a gain of 1.025 V/A. For the pulse tests, the 1.0 ohm resistor was bypassed by two paralleled high-current, low-inductance relays (OMRON G9TB-U1ATH-EDC12) for a total resistance of 0.025 ohms. The transition from high-gain to low-gain mode was achieved by shorting out a portion of resistors with parallelly-connected high-current relays (Fig. 5 and Fig. 6(c)). Both current shunt resistors and current sense resistor relays were installed inside the thermal chamber. The shunt-resistor voltage was fed out of the thermal chamber via coaxial cable to the multiplexer (NI PXI 2593, 500MHz bandwidth) where the sensed current signal from the MOV under test is connected to the oscilloscope for display.

As shown in Fig. 6(a), a medium-voltage, low-current Magna-Power XR6000DC power supply was connected to the test circuit box that hosted all relays and switches. These programmable relays determined which test was to be performed for which MOV. The MOVs under test were all enclosed in a thermal chamber that kept their operational temperatures around 65 °C. There were nine 2.2 kV-rated MOV specimens that resided within the thermal chamber simultaneously. After the failure of MOV #8 at around 30% progress of pulse endurance test, MOV #10 replaced MOV #8 to continue the following endurance tests. The MOVs under test were customized versions of Eaton VariSTAR^{TM} MOVs in UltraSIL® series [31]. The metal-oxide ceramic discs in MOVs had 19 mm in thickness and 70 mm in diameter, and the disc was terminated by 3 mm thick aluminum plates and then encapsulated in a 1.5 mm thick protective insulation layer. A cut-out photo of MOV under test will be given in Section V.

The MOV evaluation tests in this study were conducted through interleaving pulse endurance tests with TOV current measurements as illustrated in Fig. 7. In this way, the health conditions of MOVs were monitored online through pulse current readings and TOV current readings over the course of endurance tests. The clamping voltage of MOVs was also

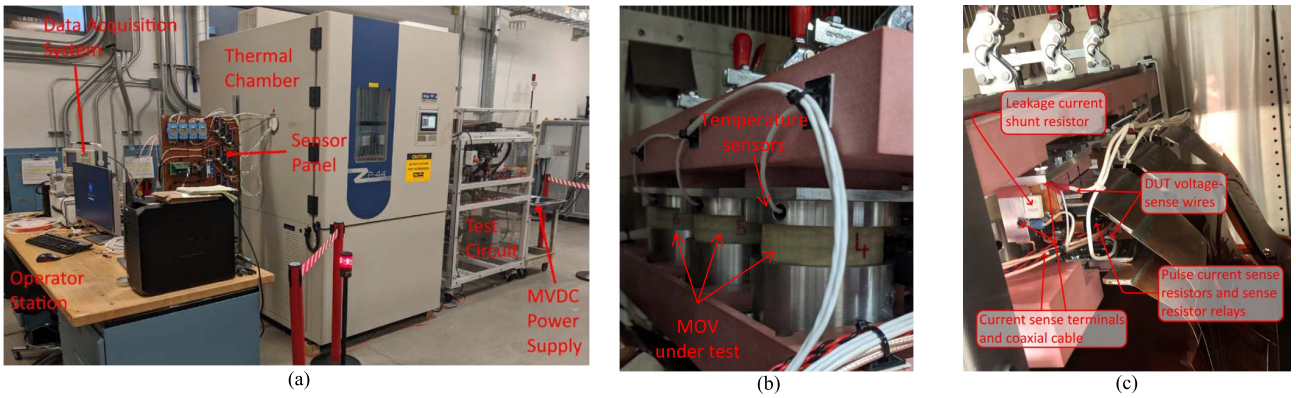

(a) (b) (c)

FIGURE 6. **Photos of (a) fully-automated testbed, (b) installations of MOV specimens inside thermal chamber, and (c) connections of busbars and current shunt resistors inside thermal chamber.**

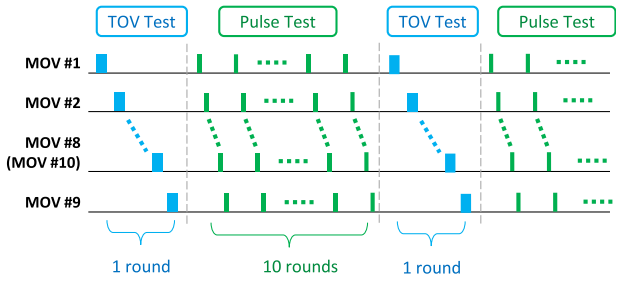

FIGURE 7. **Illustration of test sequence on MOVs and the interleaving procedure of TOV current tests with pulse current tests.**

collected from pulse endurance tests as a degradation indicator. Specifically, there was one round of TOV tests followed by ten rounds of pulse tests repetitively, and the MOVs were tested one after another in every round of pulse or TOV tests. A short period of waiting time was inserted between two pulses to allow the pulse inductor cooling down and to ensure that the power dissipation of the MOV-under-test would not lead to a significant temperature rise inside the thermal chamber. The configuration of the pulse circuit relays, charging of the capacitor, executing the test, and recording the data took about 1 minute per test. That meant a MOV would receive a pulse approximately every nine minutes. This time interval of nine minutes is significantly shorter than the interruption intervals of DCCBs under normal operations. Therefore, the MOV evaluation tests of this study are accelerated lifetime testing with frequent energy discharges and high thermal stresses on MOVs.

B. PULSE ENDURANCE TEST CIRCUIT AND PROCEDURES

The sub-circuit for pulse endurance tests is shown in Fig. 8(a). The pulse discharge relay is omitted in the sub-circuit as there is a safety switch that stays open during pulse endurance tests, and for the sake of simplicity, only MOV #1 with its affiliated components is illustrated in Fig. 8(a).

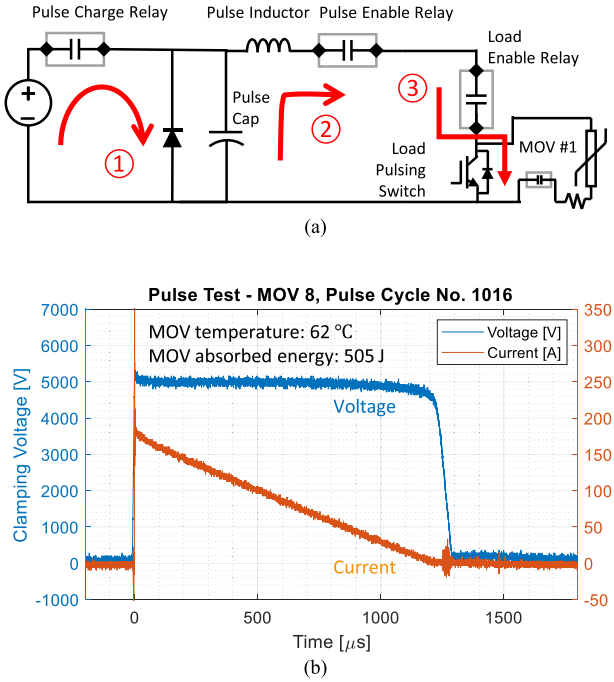

FIGURE 8. **(a) Sub-circuit diagram of pulse endurance test setup. (b) An example of DCCB-derived clamping voltage and pulse current waveforms from pulse endurance tests (for MOV #8, the 1016th pulse test, raw measurement data).**

To generate the DCCB-derived pulse current waveforms as i_{Ib} during $t_4 \sim t_5$ in Fig. 2, the pulse endurance test setup was operated as follows. Firstly, the pulse charge relay was closed to let the 6 kV, 1.3 A DC power supply charge the 3.5 kV, 700 μF pulse capacitor up to approximately 1.65 kV. Secondly, the pulse charge relay was opened before the pulse enable relay was closed. Thirdly, as illustrated in Fig. 8(a), the load enable relay, the pulse enable relay, and then the load pulsing switch closed sequentially to transfer energy from the pulse capacitor to a $L = 35.6$ mH pulse inductor. The current of pulse inductor would reach approximately $I_{peak} = 170$ A. Fourthly, the load pulsing switch was gated

off when the pulse capacitor voltage reached zero, so the 170 A-peak pulse current was commutated through MOV #1 for the pulse current test. Assuming all inductor energy was transferred to the MOV under test and neglecting the stray impedance, the following equation could be established:

$$\frac{1}{2}LI_{peak}^2 = \frac{1}{2}V_{clamp}I_{peak}t_{pulse} \tag{1}$$

where $L = 35.6$ mH was the pulse inductance, $I_{peak} = 170$ A was the inductor current before pulse discharge, $V_{clamp} = 5$ kV was the MOV clamping voltage at 170 A current conduction according to the MOV datasheet, and $t_{pulse} = 1250\mu s$ was the estimated pulse duration.

The pulse current readings through MOVs were measured with the dual-range current shunt resistors in their low-gain modes. The time-domain waveforms of voltage and current over MOVs were recorded to verify the energy absorbed by the devices under test, they also illustrated how the clamping $V-I$ characteristics might change over the lifetime of MOVs.

Fig. 8(b) shows a set of DCCB-derived waveforms with the 170 A-peak pulse current and the 5 kV-peak clamping voltage for pulse endurance tests. Both curves in Fig. 8(b) were raw readings from the 1016th pulse test of MOV #8 over a time span of 1.25 ms. The MOV temperature was 62 °C during the test, and the total energy dissipated in this pulse test was 505 J. This 500 J energy was purposely selected as the worst-case scenario to be absorbed by a single MOV in the DCCB prototype, considering there would be a total of 36 MOVs installed together in the DCCB prototype to absorb the total fault energy during one switching event. Hence, the pulse endurance tests were designed to evaluate how many worst-case events the MOV specimens could reliably endure under DCCB operations.

C. TOV CURRENT TEST CIRCUIT AND PROCEDURES

The sub-circuit for TOV current measurements is shown in Fig. 9(a). The TOV discharge relay is omitted and for simplicity, only MOV #1 is shown in the sub-circuit.

In order to measure the TOV current under 4 kV system voltage, the TOV test setup was operated as follows. Firstly, the TOV capacitor was charged to 4 kV by the MVDC power supply. This 4 kV was the hold-off voltage over one IGBT cell in the 12 kV DCCB (Fig. 4). Secondly, both the TOV test enable switch and the load enable relay closed, so the 4 kV quasi-constant voltage was applied onto the MOV-under-test for 100 ms. This 100 ms was the time interval between the current interruption in DCCB and the opening of galvanic disconnect contactor. The TOV current through the MOV under 4 kV voltage was measured by dual-range current shunt resistors in their high-gain modes. A low-pass filter whose cutoff frequency was 1/50 of sampling frequency (50 kHz) was used to filter out the unwanted high-frequency noise as shown in Fig. 9(b). The average value over the last 45 ms of filtered TOV current readings was calculated as the representative value for the TOV test according to Fig. 9(b).

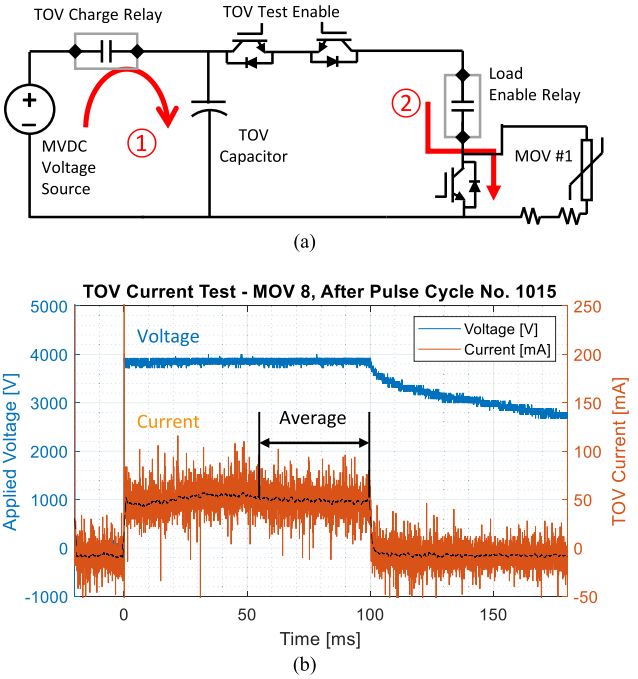

FIGURE 9. **(a) Sub-circuit diagram of TOV current test setup. (b) An example of DCCB-derived TOV current waveforms (raw and filtered) under 4 kV system voltage, and this TOV test was performed after the 1015th pulse test for MOV #8.**

TABLE 2. **Testing criteria of pulse tests and TOV tests.**

Test	Driving Signal	Test Criteria to Detect MOV Failure
Pulse	170 V peak pulse current	Conduction time > 1.5 ms
TOV	4 kV DC voltage	TOV current increase > 67%

Collectively, the driving signals and MOV failure criteria of pulse endurance tests and TOV tests are summarized in Table 2. The MOV failure criteria are summarized from MOV test results and failure analyses to be presented in following section. For better clarifications, the performed TOV current tests had replicated the hold-off processes during DCCB reclosing events, i.e., the applied voltage over MOVs dropped from 4 kV to zero without a closely preceding current pulse. In contrast, the 4 kV hold-off processes during DCCB breaking events, as shown in $t_5 \sim t_6$ of Fig. 2, happened directly after a current pulse event through MOVs. Although both hold-off processes shared the same 4 kV TOV voltage, it was observed experimentally that the TOV current might be lower immediately after a pulsed energy event. Due to the limitations of the test setup, only the TOV current from the hold-off processes in DCCB reclosing events was collected. Fig. 9(b) shows the TOV current measurements (raw and filtered) from MOV #8 taken after the 1015th pulse test.

IV. EXPERIMENTAL RESULTS

A. CLAMPING VOLTAGE FROM PULSE ENDURANCE TESTS

There were two major objectives for pulse endurance tests in this study: one was to test the endurance of MOVs under

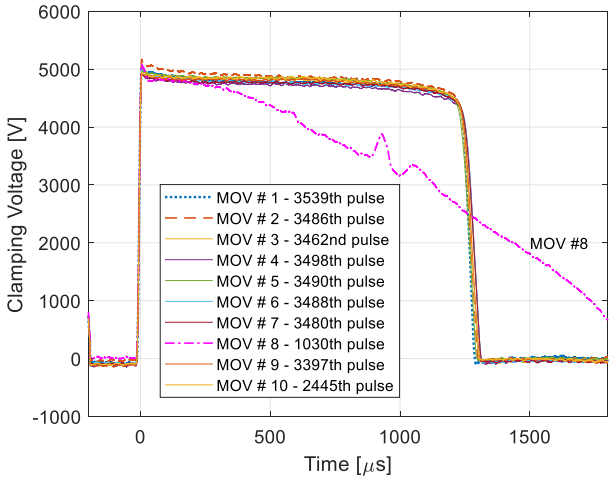

FIGURE 10. Measured clamping voltage waveforms of 10 MOVs in their last pulse test. Most MOVs had successfully survived over 3000 pulses except the MOV #8, which failed at its 1030th pulse.

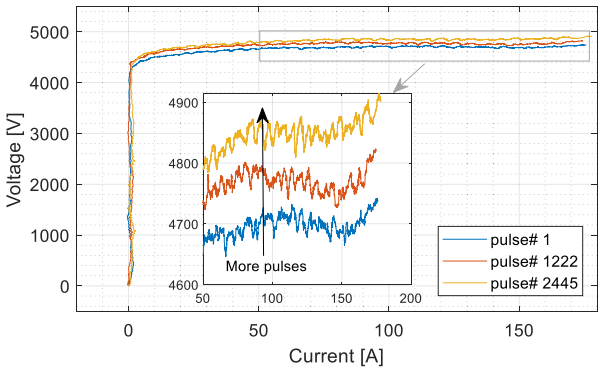

FIGURE 11. Measured variations in $V - I$ characteristics of MOV #10.

worst-case energy absorption scenarios, the other was to check if the MOV clamping voltage would significantly rise after the endurance tests. The IGBT modules in the 12 kV DCCB prototype could only withstand 5.5 kV of transient overvoltage. Therefore, if the clamping voltage of MOVs rose over 5.5 kV as the pulse endurance tests went along, it was considered an alarming sign, which calls for redesigning MOV structures.

Out of the ten MOVs under test, eight had endured around 3500 pulses without failure according to Fig. 10, one failed at its 1030th pulse (MOV #8), and a new MOV substituted the failed one and went through the remaining 2445 pulses (MOV #10). As illustrated in Fig. 10, the nonuniformity of peak clamping voltage of survived MOVs was below 4%. Here, the nonuniformity among MOVs was defined as the maximum clamping voltage (MOV #2) over the minimum clamping voltage (MOV #4) at peak pulse current. The only MOV that failed the pulse endurance test was the MOV #8 at its 1030th pulse test. More details about this failure will be provided in Section V.

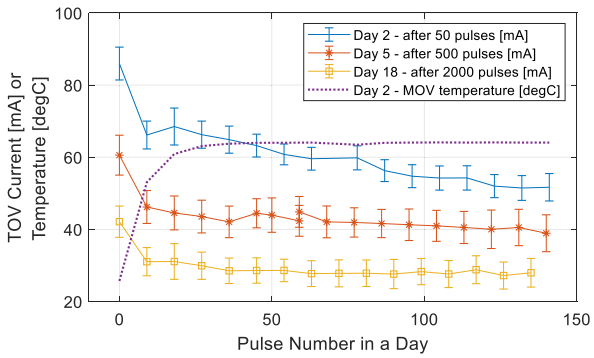

FIGURE 12. Measured TOV current of MOV #10 in three separate days of test. The MOV temperature measured at Day 2 of MOV #10 is also provided.

The clamping voltage of MOVs slightly increased as more pulses were applied, just like the trend shown in the $V - I$ characteristics of Fig. 11. The responses of MOV #10 were recorded from the very first pulse to about 2500 pulses being applied to MOV #10. By comparing the clamping voltage waveform obtained in the last pulse with the very first pulse of MOV #10 in Fig. 11, a slight 3% increase was found in its $V - I$ characteristic. This tendency matched with similar MOV tests for DCCB applications in [12], while the changes in clamping voltage measurements in this study were much less significant.

Similar to the common practice as presented in [32], most MOVs could be considered as having passed the pulse tests, because the deviations of their clamping voltage were less than 5% after the exposure to 3500 consecutive, DCCB-derived surges in the pulse tests.

B. TOV CURRENT

Even though the TOV current rating is not provided in most MOV datasheets, it is an important design parameter for DCCB applications as discussed in Section II.B. If the collective TOV current from 36 MOVs in the DCCB prototype gets too large to be interrupted by the galvanic disconnect contactor, the MOVs will stay in the TOV region of $V - I$ curve until overheating. In this study, a vacuum interrupter with copper-tungsten contacts is thus chosen to break a total TOV current of several amperes in DCCB tests.

During MOV endurance tests, the measurements of TOV current waveforms under DCCB-derived, 4 kV-constant voltage started at the beginning of each day and then continued after every ten rounds of pulse tests in all MOVs as illustrated in Fig. 7. An average value was extracted from every TOV test as the representative data in the figures of this subsection according to Fig. 9(b).

A decreasing TOV current over time was a peculiar phenomenon observed in this study. The TOV current data of MOV #10 obtained within three different days is shown in Fig. 12. The data is sorted by time in each day with the first TOV test of the day being named "pulse number 0 in

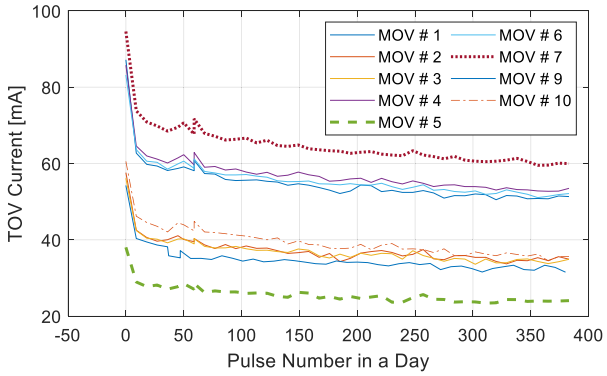

FIGURE 13. Measured TOV current of 9 MOVs in a same day. There had been about 1500 pulses applied on MOV #1 to MOV #9 and about 500 pulses applied on MOV #10 before that day of test.

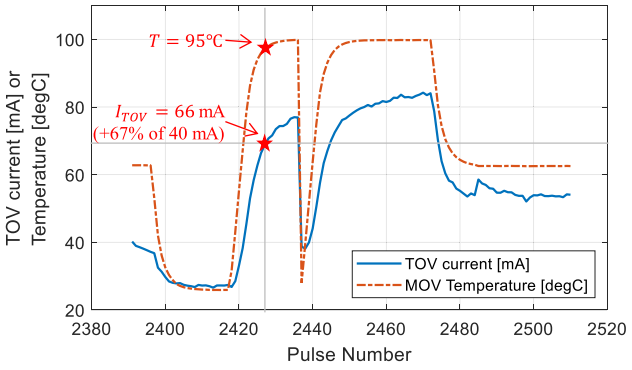

FIGURE 14. Temperature dependency of measured TOV current in MOV #10.

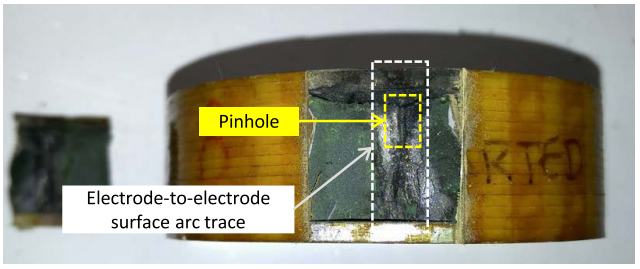

FIGURE 15. Cut-out photo of MOV #8 which failed at its 1030th pulse test. The shunt conductive path from the top to the bottom electrode can been observed with a pinhole at its top.

a day''. According to Fig. 12, these ''first data points'' of three different days were also the peak values of that day, and subsequent TOV measurement values decreased in consecutive pulses. Although the TOV current restored to a peak value after rested overnight, the TOV current peaks shifted downward day after day. For the MOV #10 under test, the first data points on Day 2 peaked at 86 mA, while the last data point on Day 18 settled around 28 mA. From a physical perspective, this decreasing but restorable TOV current might be affected by the charge trapping and recombination processes in grain boundary areas of zinc-oxide ceramic [10], [30]. This significant reduction in TOV current over applied pulses forms a distinct contrast to the degradation trend of leakage current, which normally relates a higher leakage current with a degraded MOV [12]. This flip of degradation trend has been illustrated with a crossover in $V-I$ curves between new and degraded MOVs at 0.01 A [33]. Moreover, attributing to the limited 100 ms duration of TOV stress, the TOV current kept a generally decreasing trend throughout tests. If the TOV stress was applied for an extended period of time, such as more than 2 s for the MOVs like [30], the TOV current could rise over time continuously and finally trigger overheating.

The variations of TOV current in ten MOVs were much larger than the variations of clamping voltage within the same set of MOVs. As shown in Fig. 13, the TOV current readings of MOV #7 were twice the TOV current readings of MOV #5, although both curves demonstrated similar downward tendencies over pulses.

As expected, the measured TOV current showed positive relationships with MOV temperatures as in Fig. 14. Compared to the normal test temperature around 65 °C the temperature of thermal tests in Fig. 14 fluctuated from 30 °C to 100 °C. Meanwhile, the TOV current measurements kept at the same pace with fluctuating temperatures. At the normal testing temperature of 65 °C, the TOV current of MOV #10 was around 40 mA according to Fig. 13 and Fig. 14. When the MOV temperature rose, the TOV current increased accordingly. If the fault detection limit was set at a 67% increase in the average TOV current as summarized in Table 2 (see details in Fig. 16), such as 66 mA for the MOV #10, the corresponding MOV temperature was 95 °C as shown in Fig. 14. Therefore, this 95 °C should be the dangerous temperature boundary that the MOV would be considered as ''failed'' if the temperature went higher.

V. FAILURE ANALYSIS

Among the ten MOVs under test, only MOV #8 failed at its 1030th pulse. In this section, the failure mode of MOV #8 is presumptively discussed and the waveforms measured right before the failure are presented. Fig. 15 is a cut-out photo of the failed MOV #8. The most significant failure mark is an electrode-to-electrode shunt conductive path left by the voltage collapse in the 1030th pulse test.

By inspecting the waveforms obtained right before the failure in MOV #8, pre-failure behaviors could be identified. At the 1030th pulse test for MOV #8, the pulse current was prolonged beyond 1.5 ms as in Fig. 16(a), while normal pulse current should return to zero within 1.25 ms like Fig. 8(b). This prolonged pulse current waveform flagged the failure during the test as summarized in Table 2. In the clamping voltage waveforms shown in Fig. 16(b), the ''turning-off'' corner started to collapse since the 1027th pulse. In the 1030th pulse, the clamping voltage curves collapsed to a triangular shape from the original rectangular shape, which was almost linear to the triangular-shape pulse current input. This degradation

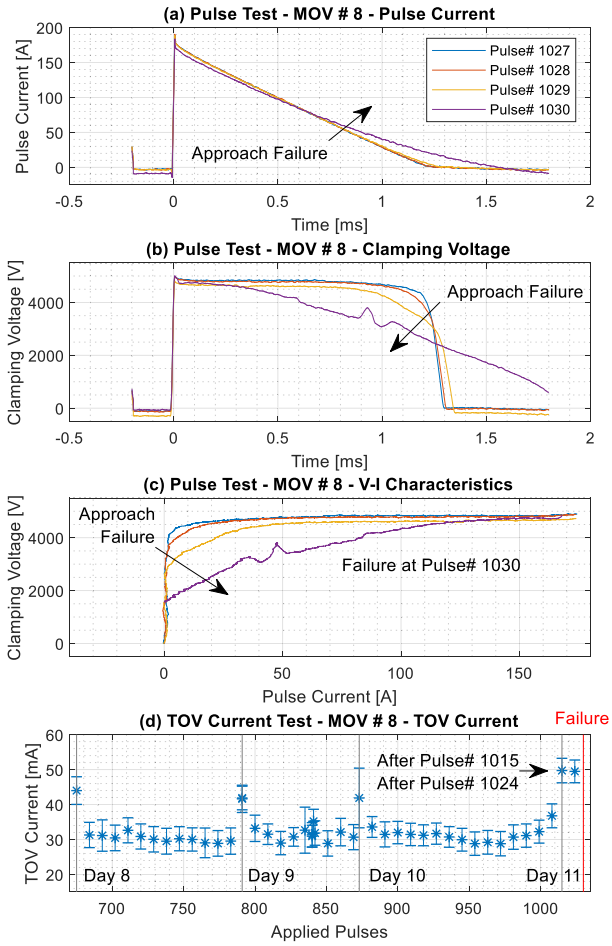

FIGURE 16. (a) Pulse current and (b) clamping voltage from pulse test measurements, (c) $V - I$ characteristics, and (d)TOV test data right before the failure of MOV #8 at its 1030th pulse test.

of nonlinearity was more clearly shown in Fig. 16(c), in which a nonlinear $V - I$ curve in the 1027th pulse degraded into a mostly-resistive one in the 1030th pulse. The loss of nonlinearity in MOV #8 was most likely caused by the formation of an electrode-to-electrode conductive channel whose trace is shown in Fig. 15. Moreover, according to Fig. 16(d), the TOV current test following the 1015th pulse was the first TOV current test of the day, which typically has an elevated TOV current (see Fig. 12). Given this, the first data point on the day of failure had a much higher TOV current value than other first data points measured on previous days, which was 67% higher than the normal TOV current of MOV #8. The TOV current after the 1024th pulse test did not significantly decrease, which differed from the second TOV test points on previous days of MOV #8 as shown in Fig. 16(d). Therefore, a sustaining 67% increase in the TOV current from its nominal value can be considered as the pre-failure signal in MOV testing as summarized in Table 2.

According to the analyses of pre-failure signals, it was reasonable to assume the devastating electrode-to-electrode conductive channel initiated with a non-devastating degradation issue like a slow overload at relatively low current density. By reviewing the cut-out photo of MOV #8 in Fig. 15, a pinhole is discovered at the top of conductive channel trace that exists on the surface of glass passivation layer. Pinhole failures usually happen at the edge of zinc-oxide ceramic stack with MOV electrodes, they are also known as punctures [11], [17], [34]. Among the common MOV failures like pinholes, cracks and flashover, pinholes often happen at a relatively lower current density like 10–100 A/cm^2 [17], and the pulse tests performed in this study fell into this current density level. So that it is reasonable to conclude that the pinhole failure is the root cause in MOV #8. Over time, the pinhole developed into an electrode-to-electrode conductive channel, which finally destroyed MOV #8. Future work will further investigate the microstructure changes inside MOVs that may cause pinhole failures.

Moreover, with further deployment of MOV-equipped switchgear, it is crucial to ensure that the standardized tests and characterization procedures can provide necessary information to switchgear designers so that they can properly select MOVs for their DCCB prototypes. Meanwhile, the design margins and lifetime expectations of MOVs should be accurately assessed. New materials, structures, analytical models, guidelines, and standards are also needed to support the research and development in this emerging application of MOVs.

VI. CONCLUSION

This paper presents the experimental investigations of MOVs as energy absorbers in DCCB applications. MOVs in DCCBs are subject to different types of stresses from traditional lightning-derived surges in power systems. In this paper, endurance tests using DCCB-derived test waveforms have been performed on a group of MOVs to investigate their changes in clamping voltage and TOV current over time. The experimental results demonstrate that most MOVs can endure around 3500 impulses with minor variations in their clamping voltage. The TOV current of all MOVs decreases with the progress of endurance tests. Only one MOV fails early in the test, which is caused by a pinhole failure with proceeding signals of a loss of nonlinearity in $V - I$ curve and an increase in the TOV current. Therefore, the lifetime estimations of MOVs in DCCBs should include new parameters like TOV current to better characterize MOVs behaviors in DCCBs.

ACKNOWLEDGMENT

This document has been reviewed by the U.S. Navy and has been granted Distribution Statement A. Approved for public release and distribution is unlimited DCN# 43-8016-21.

The authors would like to acknowledge Mike Ramarge, an Engineering Manager–Arresters, Eaton Power Reliability Division for supplying the MOVs for these tests and for his guidance and support in the writing of this paper.

DISCLAIMER

The views and conclusions contain herein are those of the authors and should not be interpreted as necessarily

representing the official policies or endorsements, either expressed or implied, of the U.S. Government.

REFERENCES

[1] C. Meyer and R. W. D. Doncker, "LCC analysis of different resonant circuits and solid-state circuit breakers for medium-voltage grids," *IEEE Trans. Power Del.*, vol. 21, no. 3, pp. 1414–1420, Jul. 2006.

[2] H. Radmanesh, S. H. Fathi, G. B. Gharehpetian, and A. Heidary, "A novel solid-state fault current-limiting circuit breaker for medium-voltage network applications," *IEEE Trans. Power Del.*, vol. 31, no. 1, pp. 236–244, Feb. 2016.

[3] R. Rodrigues, Y. Du, A. Antoniazzi, and P. Cairoli, "A review of solid-state circuit breakers," *IEEE Trans. Power Electron.*, vol. 36, no. 1, pp. 364–377, Jan. 2021.

[4] D. Jovcic, M. Zaja, and M. H. Hedayati, "Bidirectional hybrid HVDC CB with a single HV valve," *IEEE Trans. Power Del.*, vol. 35, no. 1, pp. 269–277, Feb. 2020.

[5] W. Wen, Y. Huang, Y. Sun, J. Wu, M. Al-Dweikat, and W. Liu, "Research on current commutation measures for hybrid DC circuit breakers," *IEEE Trans. Power Del.*, vol. 31, no. 4, pp. 1456–1463, Aug. 2016.

[6] B. Xiang *et al.*, "Study on the parameter requirements for resistive-type superconducting fault current limiters combined with mechanical DC circuit breakers in hybrid AC/DC transmission grids," *IEEE Trans. Power Del.*, vol. 35, no. 6, pp. 2865–2875, Dec. 2020.

[7] *IEEE Standard for Metal-Oxide Surge Arresters for AC Power Circuits (>1 kV)*, IEEE Standard C62.11-2012, 2012.

[8] S. M. Seyyedbarzegar and M. Mirzaie, "Thermal balance diagram modelling of surge arrester for thermal stability analysis considering ZnO varistor degradation effect," *IET Gener., Transmiss. Distrib.*, vol. 10, no. 7, pp. 1570–1581, May 2016.

[9] J. He, J. Lin, W. Liu, H. Wang, Y. Liao, and S. Li, "Structure-dominated failure of surge arresters by successive impulses," *IEEE Trans. Power Del.*, vol. 32, no. 4, pp. 1907–1914, Aug. 2017.

[10] Z. Topcagic, M. Mlakar, and T. E. Tsovilis, "Electrothermal and overload performance of metal-oxide varistors," *IEEE Trans. Power Del.*, vol. 35, no. 3, pp. 1180–1188, Jun. 2020.

[11] N. A. Belda, R. P. P. Smeets, and R. M. Nijman, "Experimental investigation of electrical stresses on the main components of HVDC circuit breakers," *IEEE Trans. Power Del.*, vol. 35, no. 6, pp. 2762–2771, Dec. 2020.

[12] M. Bröker and V. Hinrichsen, "Testing metal–oxide varistors for HVDC breaker application," *IEEE Trans. Power Del.*, vol. 34, no. 1, pp. 346–352, Feb. 2019.

[13] J. He, *Metal Oxide Varistors: From Microstructure to Macro-Characteristics*. Hoboken, NJ, USA: Wiley, 2019.

[14] C. Xu *et al.*, "Lightning impulse protection for grid-connected solid-state transformers," in *Proc. IEEE Energy Convers. Congr. Expo. (ECCE)*, Oct. 2020, pp. 6057–6064.

[15] Y. He, B. Wei, Z. Fu, M. Dai, and J. Liu, "MOV failure modes and microstructural characteristics under operating duty tests with multiwaveform multipulse currents," *IEEE Trans. Power Del.*, vol. 33, no. 5, pp. 2274–2283, Oct. 2018.

[16] M. N. Tuczek and V. Hinrichsen, "Recent experimental findings on the single and multi-impulse energy handling capability of metal–oxide varistors for use in high-voltage surge arresters," *IEEE Trans. Power Del.*, vol. 29, no. 5, pp. 2197–2205, Oct. 2014.

[17] N. Tsukamoto and M. Ishii, "Repetitive impulse withstand performance of metal–oxide varistors," *IEEE Trans. Power Del.*, vol. 32, no. 4, pp. 1674–1681, Aug. 2017.

[18] *IEEE Standard for Test Methods and Performance Values for Metal-Oxide Varistor Surge Protective Components*, IEEE Standard C62.33, 2018.

[19] Y. Lee and Y. S. Lee, "A low-cost surge current detection sensor with predictive lifetime display function for maintenance of surge protective devices," *Sensors*, vol. 20, no. 8, p. 2310, Apr. 2020.

[20] P. Hock, N. Belda, V. Hinrichsen, and R. Smeets, "Investigations on metal-oxide surge arresters for HVDC circuit breaker applications," in *Proc. INMR World Congr.*, 2019, pp. 20–23.

[21] Z. Zhang *et al.*, "Lifetime-based selection procedures for DC circuit breaker varistors," *IEEE Trans. Power Electron.*, early access, May 24, 2022, doi: 10.1109/TPEL.2022.3177158.

[22] L. Montanes, M. Garcia-Gracia, M. Sanz, and M. A. Garcia, "An improvement for the selection of surge arresters based on the evaluation of the failure probability," *IEEE Trans. Power Del.*, vol. 17, no. 1, pp. 123–128, Jan. 2002.

[23] C. Xu, T. Damle, and L. Graber, "A survey on mechanical switches for hybrid circuit breakers," in *Proc. IEEE Power Energy Soc. Gen. Meeting (PESGM)*, Aug. 2019, pp. 1–5.

[24] C. Franck and R. Smeets, "Technical requirements and specifications of state-of-the-art HVDC switching equipment," CIGRE WG A3/B4.34, Paris, France, Tech. Rep. 683, 2017.

[25] C. Xu *et al.*, "Piezoelectrically actuated fast mechanical switch for MVDC protection," *IEEE Trans. Power Del.*, vol. 36, no. 5, pp. 2955–2964, Oct. 2021.

[26] *IEEE Guide for the Application of Metal-Oxide Surge Arresters for Alternating-Current Systems Amendment 1: Aupplement to Consider Energy Handling Capabilities*, IEEE Standard C62.22, 2013.

[27] J. Magnusson, R. Saers, L. Liljestrand, and G. Engdahl, "Separation of the energy absorption and overvoltage protection in solid-state breakers by the use of parallel varistors," *IEEE Trans. Power Electron.*, vol. 29, no. 6, pp. 2715–2722, Jun. 2014.

[28] X. Zhang, Z. Yu, Z. Chen, Y. Huang, B. Zhao, and R. Zeng, "Modular design methodology of DC breaker based on discrete metal oxide varistors with series power electronic devices for HVdc application," *IEEE Trans. Ind. Electron.*, vol. 66, no. 10, pp. 7653–7662, Oct. 2019.

[29] M. Zaja and D. Jovcic, "Enhancing reliability of energy absorbers in DC circuit breakers," in *Proc. IEEE Power Energy Soc. Gen. Meeting (PESGM)*, Aug. 2020, pp. 1–5.

[30] T. E. Tsovilis and Z. Topcagic, "DC overload behavior of low-voltage varistor-based surge protective devices," *IEEE Trans. Power Del.*, vol. 35, no. 5, pp. 2541–2543, Oct. 2020.

[31] *UltraSIL Polymer-Housed VariSTAR Surge Arresters 5 kA and 10 kA Class 1 IEC 60099-4 for MV Systems to 36 kV, CA235029EN*, Eaton, Dublin, Ireland, 2016.

[32] M. Mashaba and K. Nixon, "Deducing metal oxide varistor life span from pulse rating curves for surges of different magnitudes," in *Proc. IEEE Int. Conf. High Voltage Eng. Appl. (ICHVE)*, Sep. 2016, pp. 1–4.

[33] D. T. Khanmiri, R. Ball, and B. Lehman, "Degradation effects on energy absorption capability and time to failure of low voltage metal oxide varistors," *IEEE Trans. Power Del.*, vol. 32, no. 5, pp. 2272–2280, Oct. 2017.

[34] M. Bartkowiak, M. G. Comber, and G. D. Mahan, "Failure modes and energy absorption capability of ZnO varistors," *IEEE Trans. Power Del.*, vol. 14, no. 3, pp. 152–162, Jan. 1999.

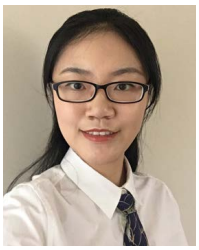

CHUNMENG XU (Member, IEEE) received the B.S. degree in electrical engineering from Xi'an Jiaotong University, Xi'an, China, in 2016, and the M.S. and Ph.D. degrees in electrical and computer engineering from the Georgia Institute of Technology, Atlanta, GA, USA, in 2019 and 2021, respectively. She is currently a Research Scientist with the ABB U.S. Research Center, Raleigh, NC, USA. Her research interests include solid state circuit breakers, multiphysical design for high power converters, and advanced protection solutions for DC power systems.

ANDREW ROCKHILL (Senior Member, IEEE) received the bachelor's degree in electrical engineering from the University of Wisconsin–Milwaukee, Milwaukee, MI, USA, and the master's and Ph.D. degrees from the University of Wisconsin–Madison, Madison, MI. He is currently a Sr. Principal Engineer with Eaton Corporations Research Labs. He is an Adjunct Instructor at the University of Wisconsin–Milwaukee, where he teaches courses on electromechanical energy conversion and power electronics. He has over 25 years of industry experience focusing on power electronics, electric machines, and power distribution and controls. With Eaton, he has been the principal investigator on multiple U.S. government funded research programs and plays a senior role in the emerging application of power electronics in the energy transition (e.g. grid and transportation). In addition to his current position, he has held senior and/or principal level positions with Plexus, American Superconductor, and GE's Global Research Center.

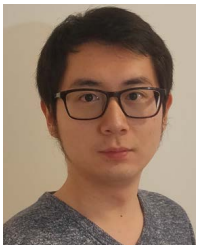

ZHI JIN (JUSTIN) ZHANG (Graduate Student Member, IEEE) received the B.A.Sc. degree (Hons.) in engineering science and the M.A.Sc. degree in electrical and computer engineering from the University of Toronto, Toronto, ON, Canada, in 2017 and 2019, respectively. He is currently pursuing the Ph.D. degree with the Georgia Institute of Technology, Atlanta, GA, USA. His research interests include the application of power electronics in power systems and cyberphysical systems security. He is the Chair of the IEEE Power Electronics Society Atlanta Chapter.

MATTHEW (MATT) BOSWORTH (Member, IEEE) received the B.S. degree in applied mathematics and computational science from Florida State University, Tallahassee, FL, USA, and the B.S. and M.S. degrees in electrical and computer engineering from the FAMU-FSU College of Engineering, Tallahassee, where he is currently pursuing the Ph.D. degree in electrical and computer engineering. At the Center for Advanced Power Systems, he works as an Associate in research with the Power Systems Group.

MARYAM SAEEDIFARD (Fellow, IEEE) received the Ph.D. degree in electrical engineering from the University of Toronto, Toronto, ON, Canada, in 2008. She is currently an Associate Professor with the School of Electrical and Computer Engineering, Georgia Institute of Technology, Atlanta, GA, USA. Prior joining Georgia Tech, she was an Assistant Professor with the School of Electrical and Computer Engineering, Purdue University, West Lafayette, IN, USA. Her research interests include power electronics and applications of power electronics in power systems.

MICHAEL (MISCHA) STEURER (Senior Member, IEEE) received the B.S. and M.S. degrees in electrical engineering from Vienna Technical University, Vienna, Austria, in 1994, and the Ph.D. degree in electrical engineering from the Swiss Federal Institute of Technology, Zürich, Switzerland, in 2001. Since 2001, he has been a Senior Researcher at the Center for Advanced Power Systems, Florida State University, where he currently leads the Power Systems Group with primarily focus on hardware-in-the-loop real-time simulation and modeling of integrated power and energy systems for all-electric ships and future terrestrial power systems. He has authored and coauthored more than 180 technical papers in the area of shipboard power systems, hardware-in-the-loop real-time simulation, fault protection, and superconductivity. He is a member of the International Council on Large Electric Systems (CIGRE) and the American Society of Naval Engineers (ASNE). He is a Senior Member of the Institute of Electrical and Electronic Engineers (IEEE), where he contributes to several working groups. He was a recipient of the 2019 ASNE Solberg Award. He chairs IEEE WG P2004 which develops a recommended practice for HIL simulations.

PETER ZELLER (Senior Member, IEEE) received the Diploma and Ph.D. degrees in electrical engineering from Vienna Technical University, Vienna, Austria, in 1993 and 2001, respectively. After his graduation, he joined ABB Switzerland, where he was the Head of the Surge Arrester Development Department. In 2001, he joined the University of Applied Sciences, where he is currently the Head of the international (English taught) electrical (energy) bachelor's and master's study programs. His research subjects are switching technology (currently e-car battery short circuit protection), contact physics, surge arrester technology and lightning protection systems, and high voltage DC technology. He is a member of the Standardization Working Group TC 81.

LUKAS GRABER (Senior Member, IEEE) received the Diploma and Ph.D. degrees in electrical engineering from ETH Zürich, Zürich, Switzerland, in 2002 and 2009, respectively. He is currently an Associate Professor with the School of Electrical and Computer Engineering, Georgia Institute of Technology, Atlanta, GA, USA. Before he joined Georgia Tech in 2015, he was with the Center for Advanced Power Systems, Florida State University, initially as a Post-Doctoral Research Associate and later as a Research Faculty Member. His research interests include superconducting power cables and fault current limiters, cryogenic power electronics, supercritical dielectric materials, ultrafast mechanical switchgear, short-circuit forces in substations, and grounding aspects of power distribution on future all-electric ships. He is a member of CIGRE, CSA, and Electrosuisse. He serves on the Board of Directors for *CSA*, an Editor for select issues for the IEEE TRANSACTIONS ON APPLIED SUPERCONDUCTIVITY, and contributes to standard committees, taskforces, as well as study committees within IEEE and CIGRE.